# Time Propagation and Spectroscopy of Fermionic Systems Using a Stochastic Technique

Kai Guther,[1,*] Werner Dobrautz,[1,†] Olle Gunnarsson,[1,‡] and Ali Alavi[1,2,§]
[1]*Max Planck Institute for Solid State Research, Heisenbergstraße 1, 70569 Stuttgart, Germany*
[2]*University Chemical Laboratory, Lensfield Road, Cambridge, CB2 1EW, United Kingdom*

(Received 6 September 2017; published 3 August 2018)

We present a stochastic method for solving the time-dependent Schrödinger equation, generalizing a ground state full configuration interaction quantum Monte Carlo method. By performing the time integration in the complex plane close to the real-time axis, the numerical effort is kept manageable and the analytic continuation to real frequencies is efficient. This allows us to perform *ab initio* calculation of electron spectra for strongly correlated systems. The method can be used as a cluster solver for embedding schemes.

DOI: 10.1103/PhysRevLett.121.056401

*Introduction.*—The time evolution of a closed interacting electronic system, having been prepared in a well-defined but entangled nonstationary state, is of considerable interest to a broad range of fields. This includes many types of electronic spectroscopy such as photoemission (PE) and inverse photoemission (IPE) [1–3], core-level [4,5] and optical spectroscopies, as well as the field of nonequilibrium dynamics [6], including dynamics in driven, time-dependent, external fields. In solid-state physics, such electronic spectroscopies play a leading role in providing information on the electronic structure of the material. In weakly correlated materials, the *GW* approximation provides a viable theoretical tool for calculating excitation energies [1,7]. In strongly correlated materials, however, theoretical studies are often limited to model systems such as the Hubbard [8] or Anderson [9] models. Efficient methods have been developed for studying such models [10,11]. However, it is not clear how these methods can be generalized to *ab initio* calculations. Here we show how this can be achieved using a time evolution method stochastically applied to *ab initio* Hamiltonians.

Time evolution of quantum systems is a notoriously difficult problem owing to the existence of a severe dynamical sign problem. For electronic systems there is another difficult sign problem due to its fermionic nature. Fundamentally, we are required to integrate the time-dependent Schrödinger equation for a many-electron system for long times. Methods based on deterministic wave function propagation, such as the Crank-Nicolson method [12], or Lanczos recursion [13,14], suffer from severe memory requirements. Quantum Monte Carlo methods (especially quantum lattice methods) typically work in imaginary frequency space [10,11], followed by analytic continuation to real frequencies. The analytic continuation is numerically highly ill conditioned, and maximum entropy (ME) methods [15,16] are usually employed. Although spectral features close to the Fermi energy can be obtained rather accurately, features farther away, e.g., satellites, are smeared out (see Supplemental Material [17]). Such satellites, however, can contain a wealth of information about the dynamics of the system. In *ab initio* models these problems are further exacerbated by the large range of energies spanned by the basis set (over numerous Hartrees) and the huge Hilbert spaces owing to the large number of virtual orbitals.

In this Letter we present an approach to this problem. We present a real-time generalization of an algorithm for calculating fermionic ground states using imaginary-time propagation. This involves the introduction of a second-order time propagator, which is implemented in a stochastic manner. This approach yields accurate time-correlation functions, but the computational cost increases exponentially, as the undamped time-evolving wave functions explore the available (exponentially large) Hilbert space. To ameliorate this problem, we introduce an adaptive variable-phase time step into the propagator, which leads to a propagation in the complex plane close to the real-time axis. This results in a slow damping, which keeps the computational cost essentially fixed (similar to a ground state calculation). Nevertheless, this gives phase information about the wave function and yields oscillatory time-correlation functions. We have developed a ME scheme, which performs analytic continuation from an arbitrary path in complex time space to real frequencies. This provides spectral functions over a broad energy range. We apply the method to benchmark systems for which numerically exact results are available, and show that these are reproduced to high accuracy at a fraction of the cost. Then we apply the algorithm to *ab initio* (atomic and molecular) systems, where comparison is made with experiment.

In *ab initio* calculations for solids, this method could be used as a cluster solver in embedding schemes like dynamical cluster approximation [10].

 

*Real-time evolution.*—Given a Hamiltonian $\hat{H}$ and an initial wave function $|\Psi(0)\rangle$, we wish to solve the time-dependent Schrödinger equation:

$$i\frac{\partial}{\partial t}|\Psi(t)\rangle = \hat{H}|\Psi(t)\rangle. \tag{1}$$

$|\Psi(t)\rangle$ gives information about various spectroscopic properties. We can see this by considering the inverse photoemission spectrum $A_{ii}(\omega)$,

$$A_{ii}(\omega) = \sum_n |\langle \Psi_n^{N+1}|c_{i\sigma}^\dagger|\Psi_0^N\rangle|^2 \delta(\omega - E_n^{N+1} + E_0^N + \mu), \tag{2}$$

where $c_{i\sigma}^\dagger$ adds an electron with spin $\sigma$ to orbital $i$ in the ground state $|\Psi_0^N\rangle$ with $N$ electrons. Here $|\Psi_n^{N+1}\rangle$ is the $n$th excited state of the $(N+1)$-electron system. $E_0^N$ and $E_n^{N+1}$ are the corresponding energies and $\mu$ is the chemical potential. The formal solution of Eq. (1) is $|\Psi(t)\rangle = \exp(-i\hat{H}t)|\Psi(0)\rangle \equiv \hat{U}(t)|\Psi(0)\rangle$. The spectrum is then given by

$$A_{ii}(\omega) = \frac{1}{\pi}\mathrm{Im}\left(-i\int_0^\infty dt e^{i[\omega+i0^+ + E_0(N)+\mu]t}\langle\Psi(0)|\Psi(t)\rangle\right), \tag{3}$$

where we have used the initial condition $|\Psi(0)\rangle = c_{i\sigma}^\dagger|\Psi_0^N\rangle$ and $0^+$ is a positive infinitesimal quantity and the calculated object is the Green's function $\langle\Psi(0)|\Psi(t)\rangle$. In a similar way, the photoemission spectrum can be calculated. These formulas are discussed in detail in Supplemental Material [17].

*Methods.*—To compute $|\Psi(t)\rangle$ accurately for long propagation times, we have adapted the full configuration interaction quantum Monte Carlo (FCIQMC) method [25–28]. This method was originally designed to stochastically project the wave function, expressed in a full Slater determinant basis $\{|D_i\rangle\}$, towards the ground state. The ground state algorithm uses a stochastic representation of the full CI wave function $\Psi = \sum_i C_i|D_i\rangle$ using signed walkers $C_i$ together with the repeated stochastic application of a short-time propagator $\hat{P}(\Delta\tau) = \mathbb{1} - \Delta\tau\hat{H}$ to the population of walkers, followed by walker annihilation at the end of each iteration. More details are given in the Supplemental Material [17].

Generalizing to the time-dependent problem, the wave function $\Psi(t) = \sum_i C_i(t)|D_i\rangle$ is represented by a collection of complex walkers, the time evolution of which is realized through the successive application of a *second-order* propagator:

$$\hat{U}_2(\Delta t) = \mathbb{1} - i\Delta t\hat{H} - \frac{1}{2}(\Delta t)^2\hat{H}^2, \tag{4}$$

where $\Delta t$ is a small time step. Thus, $\Psi(t+\Delta t) = \hat{U}_2(\Delta t)\Psi(t)$. This approach preserves the norm of the wave function to order $\mathcal{O}(\Delta t^4)$ per step and $\mathcal{O}(\Delta t^3)$ in total, which is found to be sufficient to allow for stable propagation for a long time, without significant norm-conservation errors. In contrast, propagation using a first-order propagator only leads to norm conservation of order $\Delta t$, which leads to a severe violation of unitarity over relevant timescales. The time evolution is implemented using a second-order Runge-Kutta algorithm. Numerical examples are provided in the Supplemental Material [17].

Although this method remains unitary to a good approximation, stochastic errors lead to a growth of the norm over time (see Supplemental Material [17]), which becomes unmanageable for large Hilbert spaces. We therefore allow the time step $\Delta t$ to acquire a phase $\alpha$,

$$\Delta t \mapsto e^{-i\alpha}\Delta t, \tag{5}$$

thereby introducing a damping in the propagator. The phase is varied dynamically to keep the number of walkers approximately constant. A small number of walkers requires a large $\alpha$, and increasing the number of walkers reduces $\alpha$. The pure real-time propagation ($\alpha = 0$) is achieved in the large walker limit. Since $\alpha \neq 0$ results in complex-time Green's functions, we have generalized the (imaginary-time) ME method [15,16] to compute $A(\omega)$ (see Supplemental Material [17]). The analytic continuation is more accurate for small $\alpha$, and robustness of the calculated spectra can be checked by comparing results for different numbers of walkers. To obtain the statistics needed for the ME method, we run several independent calculations.

Compared with the finite temperature Matsubara (imaginary-time) formalism, this leads to three advantages. (i) The ME method gives a more detailed spectrum, since the time path is rather close to the real axis, rather than along the imaginary axis. (ii) In each spectral calculation we shift $\mu$ so that the peak closest to $\mu$ is located at $\mu$. Since ME is most accurate close to $\mu$, this improves the accuracy. (iii) For a given $\mathbf{k}$, the weight of the PE and IPE spectra may be very different. By performing the PE and IPE calculations separately, we obtain a comparable relative standard deviation in both cases, in contrast to the Matsubara formulation. These aspects are discussed in Supplemental Material [17] and illustrated in Fig. 1(c).

*Application to the Hubbard model.*—As a first example, we consider the fermionic Hubbard model [8]. It is defined by the Hamiltonian $H = -t\sum_{\langle i,j\rangle\sigma} c_{i\sigma}^\dagger c_{j\sigma} + U\sum_i n_{i\uparrow}n_{i\downarrow}$. We consider a two-dimensional square lattice with periodic boundary conditions.

We apply the method to an 18-site cluster (18A in the notation of Betts *et al.* [30]) at half filling, which is among the largest Hubbard systems whose Green's function can be calculated numerically exactly using Lanczos recursion

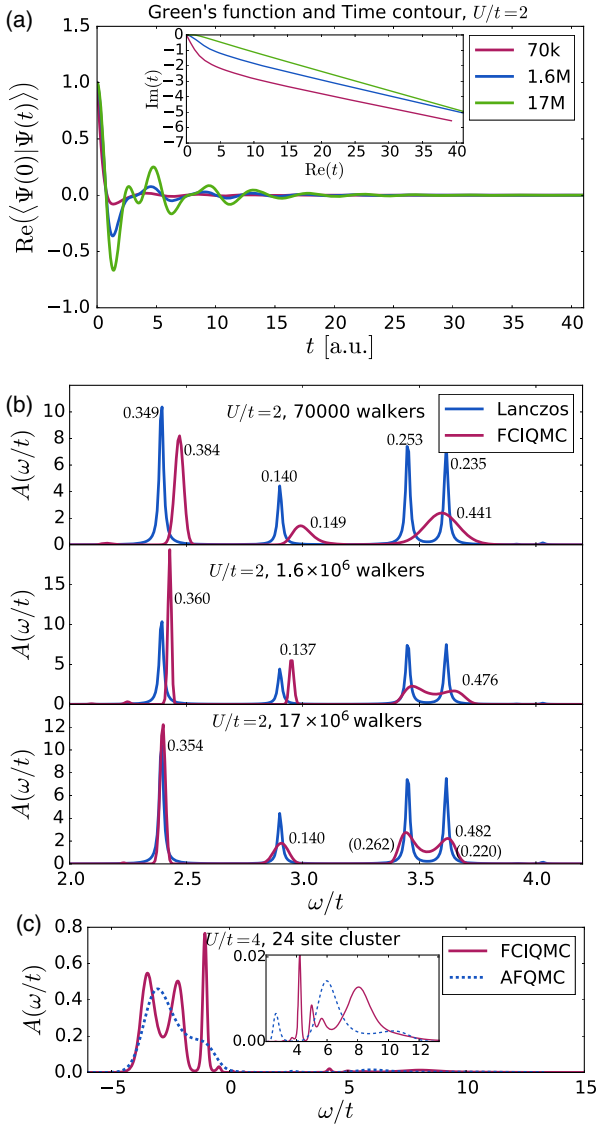


FIG. 1. (a) Time evolution of $\mathrm{Re}\langle\Psi(0)|\Psi(t)\rangle$ and contour in complex time and (b) corresponding photoemission spectra (for $\mu = 0$) for the time evolution using 70 000, $1.6 \times 10^6$, and $1.7 \times 10^7$ walkers for the 18-site Hubbard model at $U/t = 2$, $k = (0, 0)$, and half filling. All calculations start from the same initial state with 350 000 walkers, and three different time contours were used leading to 70 000, $1.6 \times 10^6$, and $1.7 \times 10^7$ walkers for longer times. The utilized time step is $10^{-3}$. Both the Lanczos and FCIQMC spectra were convoluted with a Lorentzian of FWHM of 0.02 to simplify visual comparison of the FCIQMC spectrum to the discrete eigenvalues obtained in the Lanczos method. The integrated weights of the peaks of the FCIQMC spectra are indicated and agree well with the weights of the discrete Lanczos spectrum, which are given in the first graph of (b). The bracketed numbers indicate the weights of not fully resolved peaks. (c) Photoemission and inverse photoemission spectra for a 24-site cluster with lattice vectors (3,3) and $(-5, 3)$ with 22 electrons at $U/t = 4$ for $k = (0, 0)$ obtained using $\sim 1.5 \times 10^8$ and $\sim 3 \times 10^7$ walkers respectively. The inverse photoemission part carries very low weight and is also shown in the inset. For comparison, the same spectrum computed by means of the Hirsch-Fye [29] auxiliary-field quantum Monte Carlo (AFQMC) calculation is displayed.

[13,31] (with a Hilbert space consisting of $\sim 2.4 \times 10^9$ determinants). To compute the Green's function, we first converge the ground state using imaginary-time FCIQMC calculation, and then perform a complex time calculation with a $\mathbf{k} = (0, 0)$ electron removed from the ground state. A plane waves basis set is used here.

Three calculations are shown in Fig. 1 for $U/t = 2$, employing 70 000, $1.6 \times 10^6$, and $17 \times 10^6$ walkers, with the corresponding time contours in the complex plane shown in the inset. Even though the resulting spectrum for the smallest walker number is qualitatively correct, it is broadened and shifted versus the Lanczos spectrum. Increasing the walker number to $1.6 \times 10^6$ gives less severe damping. The peaks are still slightly displaced compared to the exact result. For $17 \times 10^6$ walkers, $\alpha$ is small ($\approx 0.12$) and the spectrum is fully resolved with the peaks in their correct positions. The agreement in the weight distribution also serves as an indicator of the impact of the walker number. The memory used here is 270 Mb per processor. This already involves significant performance-memory trade-offs, such that a single replica of this calculation can be run with less than 800 Mb total memory, more than a factor of 70 smaller than for the exact diagonalization.

Figure 1(c) shows the PE and IPE spectra for a 24-site cluster with 22 electrons (24E in the notation of Betts *et al.* [30]). This illustrates that calculations can be performed for doped systems and for much larger Hilbert spaces ($\sim 6 \times 10^{12}$) than exact diagonalization. For the IPE spectrum, the main quasiparticle peak and the main satellite peak at higher energies are well resolved. This spectrum is highly difficult to compute since the initial wave function is highly multiconfigurational, as it is obtained by eliminating the Hartree-Fock determinant keeping a very high number of leading determinants with similar weight. For the PE spectrum, both the main quasiparticle peak as well as two satellite peaks can be clearly identified. As a comparison, we show results using the Hirsch-Fye method [29], based on the Matsubara formalism for $T = 0.2t$. The Hirsch-Fye PE spectrum is consistent with the FCIQMC spectrum, but the peaks are not resolved. This is due to factors (i) and (ii) above (performing analytical continuation from imaginary times and not being able to shift the peak at $-2.5t$ to 0). The weight of the IPE spectrum is only 0.035 and the relative standard deviation about a factor of 25 larger for the part of the Green's function relevant for IPE than for the PE relevant part [(iii) above].

*Application to ab initio systems.*—We employ the scheme for *ab initio* systems, namely the carbon atom and the carbon dimer at equilibrium distance. Here, the Hamiltonian is the molecular Hamiltonian in the Born-Oppenheimer approximation,

$$H = \sum_{p,q,\sigma} h_q^p c_{p\sigma}^\dagger c_{q\sigma} + \sum_{p,q,r,s,\sigma\tau} V_{qp}^{rs} c_{r\sigma}^\dagger c_{s\tau}^\dagger c_{p\tau} c_{q\sigma}, \quad (6)$$

where $h_q^p$ contains the one-body integrals of the Schrödinger Hamiltonian, and $V_{pq}^{rs}$ the two-body Coulomb integrals of the electron-electron interaction. We used the cc-pV$X$Z basis sets with $X = \mathrm{T}, \mathrm{Q}$ (referred to as V$X$Z in the following), containing 28 and 54 functions per atom, respectively, in the frozen-core approximation. The required Hamiltonian integrals were computed over restricted Hartree-Fock orbitals using MOLPRO [32].

For the carbon atom, we show the multiplet structure of the ground state in Fig. 2, obtained over a trajectory of 1600 a.u. of time.

Because of the small system size, we performed the propagation in pure real time, with a time step of $\Delta t = 5 \times 10^{-3}$. A small constant damping with a decay constant of 3 mH is applied that has negligible influence on the spectral function, but reduces the growth of walkers and allows for longer propagation times. The cation ground state energy from the ground state computation for the preparation of the initial state is $E_0^{N-1} = -37.3706\mathrm{H}$, which gives an ionization energy of 420 mH, agreeing reasonably well with the experimental finding of 413.8 mH [33]. The inset of Fig. 2 shows the oscillations of the overlap $\langle \Psi(0)|\Psi(t)\rangle$ and corresponding spectra. The resulting excitation energies agree fairly well with experiment.

Next, we consider spectral functions of a prototypical strongly correlated molecule, the carbon dimer at equilibrium distance. To target specific states, we simulate photoabsorption (PA) spectroscopy. To do so, the initial $^1\Sigma_g^+$ state is prepared by performing a ground state calculation on the neutral carbon dimer using FCIQMC calculations, and then applying the single excitation operator $c_i^\dagger c_j$ on the resulting walker population. Specifically, we consider the excitations from $1\pi_u$ to the $3\sigma_g$ and the excitation from $2\sigma_u$ to $3\sigma_g$. The former couple to $\Pi_u$ states, while the latter couple to $\Sigma_u^+$ states. Since the excitations generate open-shell determinants, the resulting spectra couple to both singlet and triplet states.

The resulting spectra for the two basis sets are shown in Fig. 3. We additionally compare to projector QMC values computed using the excited-state i-FCIQMC method [34] and using the ground state energies calculated in Ref. [35] as references. The involved Hilbert spaces contain, respectively, $10^{10}$, $10^{12}$ Slater determinants. Sharply resolved peaks which correspond to $^3\Pi_u$, $^3\Sigma_u^+$, $^1\Pi_u$, $^1\Sigma_u^+$ could be identified. We also performed photoemission and inverse photoemission calculations for the $C_2^-$ and $C_2^+$, respectively; the resulting energies for the excited states of the neutral $C_2$ are listed in Fig. 3. We find that the inverse photoemission spectra feature the lowest stochastic error while the photoemission results have a higher error. A rotation of time in the complex plane by an angle of $\alpha$ in the range [0.1, 0.2] is applied. The dependence of the spectra on the basis set is in line with the known basis-set dependence of relative energies in molecular systems, for example, ionization energies and electron affinities from FCIQMC quantum chemical studies [26,36,37]. The vertical transition energies obtained here are larger than the experimentally observed values. A previous analysis by Holmes *et al.* [38] of the excited-state potential

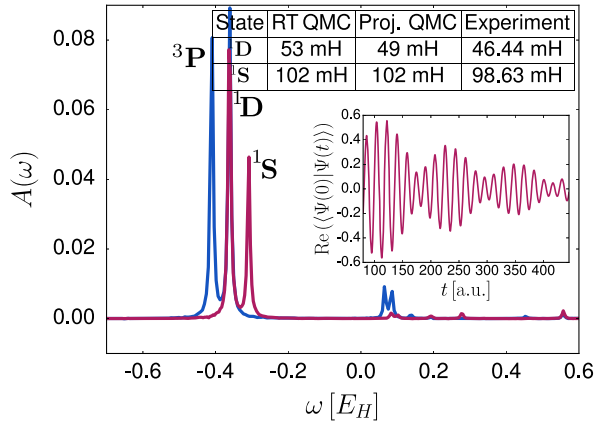


FIG. 2. Atomic multiplet of the carbon atom, obtained from two distinct initial states created by adding a $2p$ electron to the cation ground state. One of the states is prepared as a singlet (red). The second state (blue) is a mixture of singlet and triplet but with $L_z \neq 0$. The time evolution is carried out for 1600 a.u. of time and the zero of the frequency axis corresponds to $-37.3706\mathrm{H}$, which is the ground state energy of the cation computed using the projective FCIQMC algorithm. The VTZ basis is used in this example. The experimental values are according to Ref. [33]. The frequency resolution is 3.9 mH. The inset shows a portion of the computed Green's function in real time.

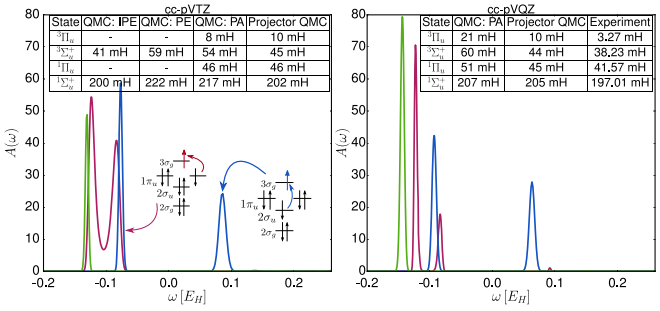


FIG. 3. Photoabsorption spectra for the carbon dimer for a single excitation from the $2\sigma_u$ to the $3\sigma_g$ (blue) and from the $1\pi_u$ to the $3\sigma_g$ (red) orbital using V$X$Z basis sets. Also shown is spectral decomposition of the FCIQMC ground state (green) as a reference. The spectra are not normalized for better display. For the VTZ basis set, we also computed $\Sigma_u$ photoemission (PE) and inverse photoemission (IPE) spectra for the $C_2^-$ and $C_2^+$, respectively. All energies and spectra are obtained with ME analytic continuation from 44–48 independent calculations. The experimental values are taken from Ref. [39]; these are also used to attribute singlet and triplet states and the $\pm$ symmetry of the $\Sigma$ states. The zero of the frequency axis is set to $-75.649\mathrm{H}$. The time step used is $\Delta t = 10^{-3}$ for the VTZ basis set and $\Delta t = 10^{-3}$ (green) and $\Delta t = 5 \times 10^{-4}$ (red and blue) for the VQZ basis set.

energy curves shows a significant effect of bond-length variation for the states considered here, indicating the likely nonvertical character of the experimental transitions.

*Conclusions.*—We have presented an efficient method for solving the time-dependent Schrödinger equation. We generalize a full configuration interaction quantum Monte Carlo method to calculations for complex times close to the real axis. We then develop a maximum entropy method for analytic continuation from complex times to real frequency. The method can be used to calculate electron spectra. The imaginary component of time strongly limits the numerical effort without a strong negative impact on the analytic continuation. We demonstrated that spectra of the Hubbard model can be obtained in good agreement with exact Lanczos calculations. We then applied the method to *ab initio* systems, the C atom, and the $C_2$ molecule, and obtained good agreement with experiment for excitation energies. The method can be used as a cluster solver in embedding schemes for solids. It can also be used to study small systems in strong external fields without any assumptions about linear response.

*k.guther@fkf.mpg.de
†w.dobrautz@fkf.mpg.de
‡o.gunnarsson@fkf.mpg.de
§a.alavi@fkf.mpg.de

[1] L. Hedin and S. Lundqvist, Solid State Phys. **23**, 1 (1970).
[2] D. W. Turner, Phil. Trans. R. Soc. A **268**, 7 (1970).
[3] F. J. Himpsel and T. Fauster, J. Vac. Sci. Technol. A **2**, 815 (1984).
[4] J. J. Pireaux, S. Svensson, E. Basilier, P.-A. Malmqvist, U. Gelius, R. Caudano, and K. Siegbahn, Phys. Rev. A **14**, 2133 (1976).
[5] P. Mills and J. L. Sullivan, J. Phys. D **16**, 723 (1983).
[6] A. Polkovnikov, K. Sengupta, A. Silva, and M. Vengalattore, Rev. Mod. Phys. **83**, 863 (2011).
[7] G. Onida, L. Reining, and A. Rubio, Rev. Mod. Phys. **74**, 601 (2002).
[8] J. Hubbard, Proc. R. Soc. A **276**, 238 (1963).
[9] P. W. Anderson, Phys. Rev. **124**, 41 (1961).
[10] T. Maier, M. Jarrell, T. Pruschke, and M. H. Hettler, Rev. Mod. Phys. **77**, 1027 (2005).
[11] E. Gull, A. J. Millis, A. I. Lichtenstein, A. N. Rubtsov, M. Troyer, and P. Werner, Rev. Mod. Phys. **83**, 349 (2011).
[12] J. Crank and P. Nicolson, Proc. Cambridge Philos. Soc. **43**, 50 (1947).
[13] B. N. Parlett, *The Symmetric Eigenvalue Problem* (Prentice-Hall, Englewood Cliffs, NJ, 1980), p. 257.
[14] T. Park and J. Light, J. Chem. Phys. **85**, 5870 (1986).
[15] R. N. Silver, D. S. Sivia, and J. E. Gubernatis, Phys. Rev. B **41**, 2380 (1990).
[16] M. Jarrell and J. Gubernatis, Phys. Rep. **269**, 133 (1996).
[17] See Supplemental Material at http://link.aps.org/supplemental/10.1103/PhysRevLett.121.056401 for a summary of the FCIQMC method, a more detailed discussion of the calculation of Green's functions and optical absorption spectra, details of the time-evolution algorithm regarding the complex time contour as well as the usage of a second order Runge-Kutta scheme, and a discussion of the ME methodology. References [18–24] are also included.
[18] C. Daday, S. D. Smart, G. H. Booth, A. Alavi, and C. Filippi, J. Chem. Theory Comput. **8**, 4441 (2012).
[19] J. J. Shepherd, G. H. Booth, A. Grüneis, and A. Alavi, Phys. Rev. B **85**, 081103 (2012).
[20] F. R. Petruzielo, A. A. Holmes, H. J. Changlani, M. P. Nightingale, and C. J. Umrigar, Phys. Rev. Lett. **109**, 230201 (2012).
[21] N. S. Blunt, S. D. Smart, J. A. F. Kersten, J. S. Spencer, G. H. Booth, and A. Alavi, J. Chem. Phys. **142**, 184107 (2015).
[22] C. Overy, G. H. Booth, N. S. Blunt, J. J. Shepherd, D. Cleland, and A. Alavi, J. Chem. Phys. **141**, 244117 (2014).
[23] L. Verlet, Phys. Rev. **159**, 98 (1967).
[24] O. Gunnarsson, M. W. Haverkort, and G. Sangiovanni, Phys. Rev. B **81**, 155107 (2010).
[25] G. H. Booth, A. J. W. Thom, and A. Alavi, J. Chem. Phys. **131**, 054106 (2009).
[26] G. H. Booth and A. Alavi, J. Chem. Phys. **132**, 174104 (2010).
[27] D. Cleland, G. H. Booth, and A. Alavi, J. Chem. Phys. **132**, 041103 (2010).
[28] G. H. Booth, A. Gruneis, G. Kresse, and A. Alavi, Nature (London) **493**, 365 (2012).
[29] J. E. Hirsch and R. M. Fye, Phys. Rev. Lett. **56**, 2521 (1986).
[30] D. D. Betts, H. Q. Lin, and J. S. Flynn, Can. J. Phys. **77**, 353 (1999).
[31] O. Gunnarsson and K. Schönhammer, in *Handbook on the Physics and Chemistry of Rare Earths*, edited by K. A. Gschneider, Jr., L. Eyring, and S. Hüfner (Elsevier, New York, 1987), Vol. 10, p. 103.
[32] H.-J. Werner, P. J. Knowles, G. Knizia, F. R. Manby, and M. Schütz, WIREs Comput. Mol. Sci. **2**, 242 (2012).
[33] V. Kaufman and J. F. Ward, J. Opt. Soc. Am. **56**, 1591 (1966).
[34] N. S. Blunt, S. D. Smart, G. H. Booth, and A. Alavi, J. Chem. Phys. **143**, 134117 (2015).
[35] D. Cleland, G. H. Booth, C. Overy, and A. Alavi, J. Chem. Theory Comput. **8**, 4138 (2012).
[36] D. M. Cleland, G. H. Booth, and A. Alavi, J. Chem. Phys. **134**, 024112 (2011).
[37] G. H. Booth, D. Cleland, A. J. W. Thom, and A. Alavi, J. Chem. Phys. **135**, 084104 (2011).
[38] A. A. Holmes, C. J. Umrigar, and S. Sharma, J. Chem. Phys. **147**, 164111 (2017).
[39] M. Martin, J. Photochem. Photobiol. A **66**, 263 (1992).